



OPEN ACCESS

EDITED BY

Yongli Wang,
Chinese Academy of Sciences, China

REVIEWED BY

R. Jayangonda Perumal,
Wadia Institute of Himalayan Geology, India
Tapan Chakraborty,
Indian Statistical Institute, India

*CORRESPONDENCE

Tao Li,
✉ litao.410@163.com

RECEIVED 30 August 2024

ACCEPTED 31 October 2024

PUBLISHED 15 November 2024

CITATION

Deng J, Li T, Feng J and Qian L (2024) Late Quaternary fluvial terrace characteristics and ages of the Pamir–Tian Shan convergence zone: indications of regional climate change and tectonic uplift.

Front. Earth Sci. 12:1488517.

doi: 10.3389/feart.2024.1488517

COPYRIGHT

© 2024 Deng, Li, Feng and Qian. This is an open-access article distributed under the terms of the [Creative Commons Attribution License \(CC BY\)](https://creativecommons.org/licenses/by/4.0/). The use, distribution or reproduction in other forums is permitted, provided the original author(s) and the copyright owner(s) are credited and that the original publication in this journal is cited, in accordance with accepted academic practice. No use, distribution or reproduction is permitted which does not comply with these terms.

Late Quaternary fluvial terrace characteristics and ages of the Pamir–Tian Shan convergence zone: indications of regional climate change and tectonic uplift

Jinhua Deng^{1,2}, Tao Li^{1*}, Jiahui Feng^{1,3} and Li Qian¹

¹State Key Laboratory of Earthquake Dynamics, Institute of Geology, China Earthquake Administration, Beijing, China, ²Sichuan Institute of Geological Engineering Investigation Group Co., Ltd., Chengdu, China, ³Railway Science and Technology Research and Development Center, China Academy of Railway Sciences Co., Ltd., Beijing, China

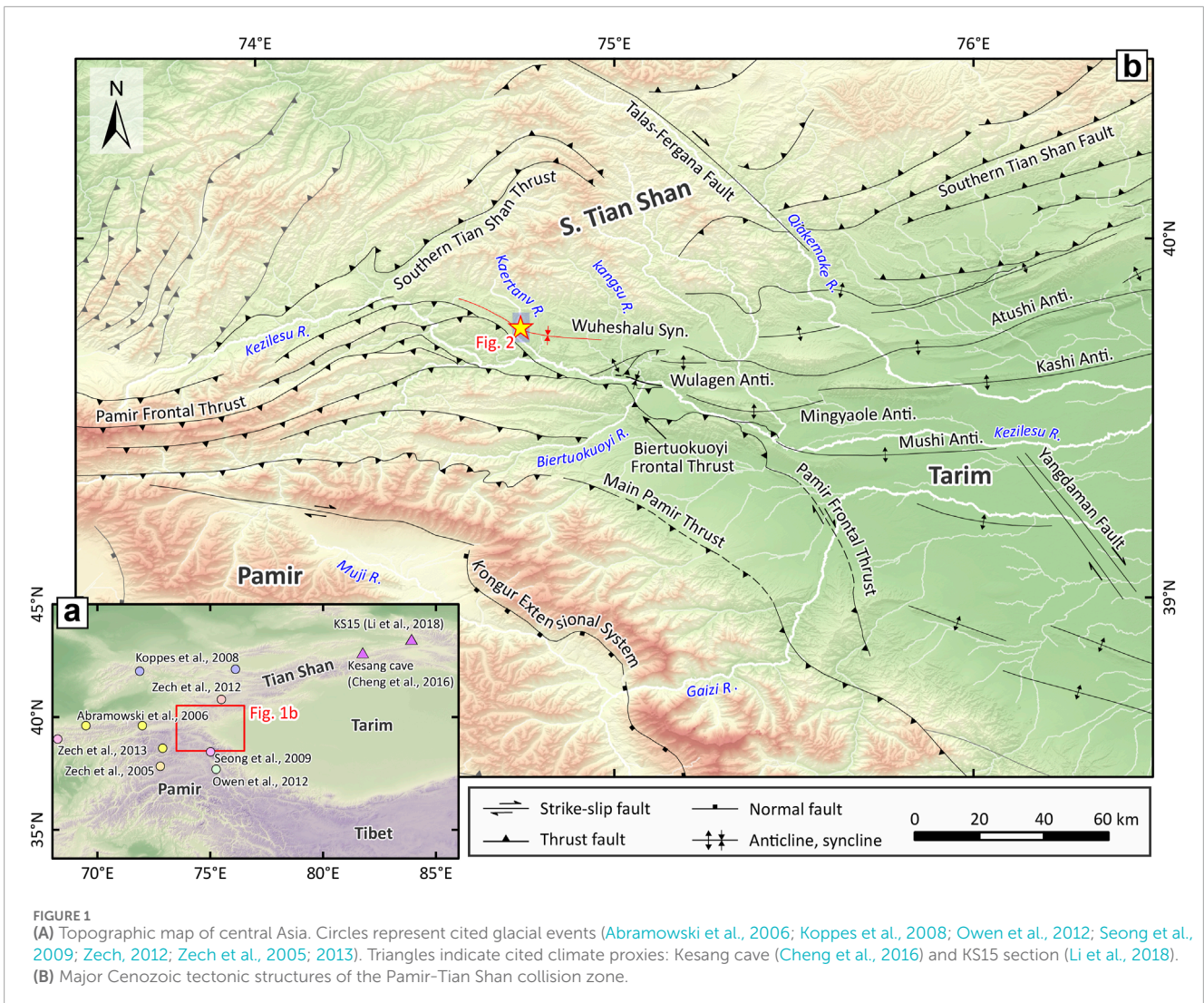
The Pamir–Tian Shan collision zone, located at the northwestern edge of the Himalaya–Qingzang orogenic belt, provides a natural laboratory for investigating the development of fluvial terraces controlled by regional climate change and tectonic uplift. In this study, we conducted geomorphological mapping and terrestrial cosmogenic nuclide ¹⁰Be dating of fluvial terraces in the Wuheshalu syncline, within the Pamir–Tian Shan collision zone. Four major fluvial terraces were identified in the Wuheshalu syncline, with ages of approximately 187, 141, 90, and 19 ka, respectively. These terraces were abandoned during three glacial-interglacial transition periods (Marine Isotope Stage 6/5 (MIS6/5), cold-to-warm transition period of MIS5, and end of MIS2 or MIS2/1) and one interglacial-glacial period (MIS7/6), and exhibit a strong correlation with regional climate change. Tectonic uplift contributed only one-third of the observed fluvial incision. These results suggest that river incision and terrace formation in the Pamir–Tian Shan collision zone are primarily driven by periodic fluctuations in climate, with a lesser contribution from tectonic uplift.

KEYWORDS

Pamir–Tian Shan, fluvial terraces, terrestrial cosmogenic nuclide ¹⁰Be exposure dating, regional climate change, tectonic uplift

1 Introduction

The sedimentary successions, origins, and structural deformation features of fluvial terraces are critical subjects within the fields of neotectonics and paleoclimatology (Bull, 1990; Dey et al., 2016; Maddy et al., 2001; Maddy et al., 2012; Veldkamp and Van Dijke, 2000; Singh et al., 2024). With the continued accumulation of field, experimental simulation, and numerical modeling evidence, a model of climate–tectonic interaction controlling terrace formation has gained widespread acceptance among the research community (e.g., Huang et al., 2014; Pan et al., 2001; Starkel, 2003). In this model, climate change dictates the timing of river aggradation (or incision) and terrace development, while tectonic uplift provides the driving force and space for



fluvial incision (Bridgland and Allen, 1996; Bridgland et al., 2004; Pan et al., 2003; Pan et al., 2009; Vandenberghe and Maddy, 2001). However, differences in location, climate, tectonic activity, and river size have led to diverse fluvial terrace genesis theories and developmental traits. Consequently, it is crucial to conduct detailed investigations of the ways in which fluvial terraces form and evolve in various settings and circumstances.

The Pamir region, located at the northwestern margin of the Himalaya-Qingzang orogenic belt, continues to experience substantial deformation owing to collision between the Indian and Eurasian plates (Figure 1A) (Chen et al., 2011; Li et al., 2019; Jayagondaperumal et al., 2018). Pamir is a frigid, high-altitude area containing large modern continental glaciers. The regional climate is mostly affected by the westerlies, resulting in notable periodic climatic variations that have occurred since the late Quaternary (Chen et al., 2008; Tao et al., 2020). Moreover, interactions between regional climate change and tectonic activity have resulted in the development of a sequence of broad, flat, and well-preserved fluvial terraces (Li et al., 2015), positioning the Pamir area as an ideal location for investigating the origin and formation processes of such terraces.

Numerous investigations have been conducted on fluvial terraces in the Pamir foreland area. For example, optically stimulated luminescence (OSL) dating of fine-grained quartz has been employed to determine the ages of fluvial terraces in the Mingyaole anticline, Wuheshalu syncline, and Muji anticline (Li et al., 2013a; 2017; Thompson et al., 2017). By comparing these ages with marine oxygen isotope curves, it has been revealed that these terraces formed during glacial-interglacial transitions, supporting the hypothesis that fluvial incision and terrace formation occur during climatic transitions. Given the problem of insufficient bleaching in fine-grained quartz, Li et al. (2015) and Thompson et al. (2018) further employed coarse-grained quartz OSL dating and terrestrial cosmogenic nuclide (TCN) ^{10}Be depth profile dating to constrain the ages of major fluvial terraces in the Mingyaole anticline and Mayikake Basin, and estimated the deformation rates of notable active structures. However, these studies primarily focused on the deformation characteristics and formation ages of terraces associated with active tectonics (e.g., active faults and folds) to constrain the growth mechanisms and deformation rates of active structures (Li et al., 2012; Li et al., 2013a; Li et al., 2017). However, there is a gap in systematic studies of the formational mechanism

of the terraces and the relative role of climate and tectonics in their formation in the Pamir–Tian Shan collision zone.

This research concentrates on the Wuheshalu syncline, which is characterized by extensive fluvial terraces and notable tectonic deformation, with the aim of determining its geomorphology and a temporal framework of their development. Initially, thorough field surveys and measurements were carried out to collect precise geomorphological data, including the spatial distribution, sequences, and sedimentary structures of the fluvial terraces. We then determined the abandonment ages of the Wuheshalu terraces using TCN ^{10}Be depth profiles and surface exposure boulder ages (Huang et al., 2019; Li et al., 2019). Finally, we conducted a comprehensive study on the interplay between fluvial terrace formation, tectonic uplift, and regional climate change, combining tectonic uplift characteristics (Li et al., 2017) and regional climate records (e.g., Berger and Loutre, 1991; Cheng et al., 2016; Li et al., 2018; Lisiecki and Raymo, 2005; Owen et al., 2012; Seong et al., 2009; Zech et al., 2013). The new data presented herein can help to clarify the tectonic evolution and incision histories of terraces in the Pamir–Tian Shan convergence zone.

2 Regional setting

The Tarim Basin, located in northwest China, is one of the major foreland basins of Central Asia (Figure 1A). It is bounded to the southwest by the Pamir Plateau, which extends northwards in a curved shape and constitutes the northwestern edge of the Himalaya orogen, with peaks >7,000 m high. To the north of the Tarim Basin, the Tian Shan stretch over 2,000 km from Uzbekistan in the west to China in the east, with a mountain belt width of 300–500 km (Figure 1A). The large-scale collision between the Indian plate and Eurasian continent has resulted in the formation of numerous fold and thrust belts and thick late Cenozoic sediments along the frontal zone of the Pamir Plateau and southern Tian Shan (Burtman and Molnar, 1993).

2.1 Climatic setting

Late Quaternary climate change in the Pamir–Tian Shan region can be inferred from Northern Hemisphere benthic cores, Greenland ice cores, regional climate records, and glacial deposits (e.g., moraines). According to climate proxies obtained from benthic cores and Greenland ice cores (Lisiecki and Raymo, 2005; Mayewski et al., 1997), global climate change since the Quaternary has exhibited cycles of 100, 41, 2.3, and 1.9 ka, controlled by Earth's orbital eccentricity, obliquity of the ecliptic, and precession. Specifically, from 2.4 to 1.1 Ma, the duration of dominant climate-change cycle was 41 ka, characterized by high frequency and low amplitude. From 1.1 to 0.7 Ma, the 41-ka cycle persisted, but with high frequency and high amplitude. Since 0.7 Ma, influenced by the 100-ka orbital eccentricity cycle, the 41-ka cycle has shown low frequency and high amplitude.

Regional indicators, such as stalagmite $\delta^{18}\text{O}$ records from Kesang Cave (Cheng et al., 2016), magnetic susceptibility data from the KS15 loess section (Li et al., 2018), and glacial advances or retreats recorded by moraines (Abramowski et al., 2006;

Koppes et al., 2008; Owen et al., 2012; Seong et al., 2009; Zech, 2012; Zech et al., 2005; Zech et al., 2013), are important for studying regional climatic variations. These indicators complement the global climate change indicators observed in benthic cores and Greenland ice cores (Figure 1A).

In recent years, the development and widespread application of TCN dating have provided precise constraints on the phases, timing, and extent of late Quaternary glaciations in the Pamir and Tian Shan regions (Owen and Dortch, 2014). Such studies have identified four major glacial advances since the late Quaternary: the penultimate glacial cycle (Marine Isotope Stage 6–8 (MIS6–8) and/or earlier, early Last Glacial (MIS4), early MIS2, and Last Glacial Maximum (LGM) (Owen et al., 2012; Seong et al., 2009). The primary factor influencing glacial advances appear to have been rapid climate change associated with Northern Hemisphere westerlies, whereas the South Asian monsoon had relatively little impact (Owen and Dortch, 2014). Seong et al. (2009) discovered multiple Holocene glacial advances in Muztagh Ata and Kongur Shan, indicating millennial-scale glacial advance events coinciding with rapid climate oscillations in the Northern Hemisphere since the global LGM (e.g., Bond et al., 2001; Mayewski et al., 2004). These glacial records have illuminated Pamir climate change and yielded important information for studying fluvial aggradation/incision and climate change.

2.2 Geological and geomorphological setting

At the northwestern end of the Himalaya–Qingzang orogenic belt, the Pamir Plateau is the western tectonic knot where the Indian plate aggressively converges with the Eurasian continent (Figure 1A) (Burtman and Molnar, 1993). Since the Cenozoic, the Pamir Plateau has experienced considerable crustal shortening, thickening, and surface uplift owing to the northward indentation of the Indian plate, pushing it approximately 300 km into the Eurasian continent (Burtman and Molnar, 1993; Cowgill, 2010). According to focal mechanism solutions, GPS velocity fields, and active tectonic surveys, the modern Pamir Plateau has been severely compressed and shortened along its northern and western borders (Chapman et al., 2017; Li et al., 2012; Zubovich et al., 2010). Along the approximately north–south trending Kongur Extensional System (KES), the central–western Pamir Plateau is currently separating from the eastern Pamir Plateau (Jay et al., 2017; Li et al., 2019; Robinson et al., 2004; Schurr et al., 2014; Thiede et al., 2013). On the northeastern Pamir Plateau, tectonic deformation since the Miocene has been dominated by the north-verging Pamir Thrust System, faults and folds within the foreland basin, dextral-slip Kashgar–Yecheng Transfer System along the eastern margin, and east–west extension along the KES (Li et al., 2017; Sobel et al., 2011; Thiede et al., 2013; Thompson et al., 2017).

The Tian Shan, located to the north of the Tarim Basin, are a crucial part of the Central Asian accretionary orogenic belt (Charvet et al., 2011; Molnar and Tapponnier, 1975) (Figure 1A). Several collisions between the Indian and Eurasian plates have resulted in the complicated tectonic evolution of the Tian Shan since the late Oligocene–early Miocene (Carroll et al., 1995; Dumitru et al., 2001; Hendrix et al., 1992; Windley et al., 1990). The southwestern

Tian Shan experienced considerable uplift at approximately 25 Ma owing to the northward indentation of the Pamir region (Sobel et al., 2006; Yin et al., 1998). With subsequent propagation in a foreland direction, multiple fold-thrust belts (Li et al., 2013b; Schärer et al., 2004) and thick late Cenozoic deposits were formed in the foreland basin (Heermance et al., 2008; Sobel et al., 2006).

The Pamir-Tian Shan thrust belt is a convergence zone where the northward-thrusting Pamir Plateau meets the southward-thrusting southwestern Tian Shan (Figure 1); its major active structures include faults (e.g., northward-thrusting Pamir and Biertuokuoyi frontal thrusts) and folds (e.g., Wuheshalu syncline and Wulagen, Mingyaole, and Mush anticlines) (Li et al., 2012; Li et al., 2013a; Li et al., 2015; Thompson et al., 2017). These structures are shortening at a rate of approximately 1–4 mm/a, whereas the deformation zone as a whole is shortening at a rate of approximately 7–10 mm/a, which matches the convergence rate of approximately 6–9 mm/a obtained from GPS velocity profiles (Li et al., 2019).

There is a large axial river system (Kezilesu River) that flows from west to east along the topographic low points of the Pamir and southern Tian Shan convergent systems (Figure 1B). Most of its water originates from glacier meltwater and atmospheric precipitation, and its basin spans 16,000 km². The Kaertanv River, a tributary of the Kezilesu River, runs through the study area. Owing to regional climatic variations and tectonic uplift, the river has down-cut in phases, resulting in well-preserved fluvial terraces being formed along its banks since the late Pleistocene.

The Wuheshalu syncline lies between the Pamir Plateau and southern Tian Shan (Figure 1B). The synclinal fold trends NW-SE in the west, shifting to nearly E-W in the east, and displays a gentle southward-verging arcuate shape and a length exceeding 50 km (Li et al., 2017). The northern and southern limbs dip approximately 50° S and 62° N, respectively. The eastern half of the syncline trends east and is relatively open and broad, whereas in its western half, the fold axis rotates to a SE trend and the syncline becomes tight and narrow in response to the northward impingement of the Pamir frontal thrust (Li et al., 2017). The southern Kaertanv River, originating in the Tian Shan, runs north-south, turns southeast along the syncline axis, and joins the eastward-flowing Kezilesu River. Lateral erosion and downcutting (the vertical erosion) by the river have created a large channel and several broad, flat fluvial terraces along the Wuheshalu syncline (Figure 1B).

3 Dating of quaternary fluvial terraces

Geomorphic surface exposure ages are essential for statistically studying Wuheshalu fluvial terrace development mechanisms. Various dating methods are commonly used in river terrace chronostratigraphy, including radiocarbon (¹⁴C), electron spin resonance (ESR), U-Th, OSL, and TCN ¹⁰Be exposure dating (Darling et al., 2012; Harkins et al., 2007; Lavé and Avouac, 2001; Perrineau et al., 2011; Wegmann and Pazzaglia, 2009; Yang et al., 2020; Singh et al., 2024). In this study, we used TCN ¹⁰Be exposure dating, including depth profile and surface gravel dating, to calculate terrace abandonment ages.

Glacial and fluvial exogenic geological processes bring subsurface rocks to the surface, where they are irradiated by cosmic rays, producing cosmogenic nuclides (e.g., ¹⁰Be, ²¹Ne,

and ²⁶Al) within mineral lattices (Lal, 1991). These nuclides accumulate throughout the exposure time of the minerals, allowing the calculation of geomorphic surface exposure ages based on the nuclide concentration accumulated in surface rocks or sediments.

We collected surface and depth profile samples for TCN ¹⁰Be analysis from major terraces within the Wuheshalu syncline. To reduce the influence of secondary transport and erosion, we selected sampling locations on well-preserved and flat terrace surfaces with minimal surface erosion (i.e., absence of substantial water channels and gullies), avoiding the effect of topographic shielding. Surface samples contained several 2 cm quartz grains and weighed >500 g. Because quartz exposed at the surface may have an initial nuclide concentration, we assumed homogeneous inheritance at a given site and rapid sedimentation across the sampling region. Therefore, we collected depth profile samples from several terraces to obtain more accurate terrace abandonment ages. Multiple samples were taken from different depths within a given vertical profile using 1 × 2 m sampling trenches that were approximately 2 m deep; these samples were also used to correct for inheritance in the surface samples.

The purification of quartz minerals from all samples was conducted at the Neotectonics and Chronology Laboratory of the Institute of Geology, China Earthquake Administration. First, gravel samples were crushed and sieved to obtain particles in the size range of 250–500 μm. Next, the samples were treated in HCl and H₂O₂ to remove carbonate minerals and organic debris, while magnetic minerals were removed using magnetic separation. The samples were then repeatedly etched with a 5% HF/HNO₃ mixture to thoroughly remove atmospheric ¹⁰Be and feldspar minerals associated with the quartz. Final purification was achieved using sodium polytungstate heavy liquid separation.

The purified quartz minerals were then processed for ¹⁰Be chemical separation at the Terrestrial Cosmogenic Nuclide Preparation Laboratory of the Institute of Crustal Dynamics, China Earthquake Administration. First, ~30 g of quartz sample was combined with a ⁹Be carrier, dissolved in HF, and heated until fully dissolved. The Be was then extracted using a cation exchange resin column, and ammonia was used to modify the pH of the post-column solution to 9, precipitating Be(OH)₂. Next, BeO was obtained by combusting this precipitate at 920°C in a muffle furnace. Finally, the BeO was combined with an equal amount of Nb powder, transferred to a Cu target, and pressed into accelerator mass spectrometry (AMS) ¹⁰Be targets.

All ¹⁰Be targets were sent to the PRIME Laboratory at the Department of Physics, Purdue University, for AMS testing. The measurement standard used was 07KNSTD (¹⁰Be half-life of 1.387 ± 0.012 Ma, and ¹⁰Be/⁹Be ratio of 2.851 × 10⁻¹²; Nishiizumi et al., 2007).

Depth profiles in this study were dated using the Monte Carlo simulator (version 1.2) in Matlab (Hidy et al., 2010). The exposure ages of the ¹⁰Be surface samples were determined using the CRONUS-Earth online calculator (version 3.0) provided by the University of Washington (<http://hess.ess.washington.edu/>), employing the LSDn production rate model (Lifton et al., 2014). The inheritance values obtained from depth profile dating were utilized to adjust the ¹⁰Be concentrations of surface samples during the computation of surface sample ages, while the effects of erosion rates were disregarded. Detailed sample information and test results are presented in Table 1.

TABLE 1 Analytical results of terrestrial cosmogenic nuclide ¹⁰Be geochronology.

Sample no.	Latitude/Longitude	Elevation (m)	Depth (cm)	Thickness (cm)	Production rate (atoms/g/a) ^a	Shielding correction	Mass qtz (g)	⁹ Be carrier (mg)	¹⁰ Be/ ⁹ Be (10 ⁻¹⁴) ^b	¹⁰ Be concentration (10 ⁴ atoms/g)
WHSL1 (depth sample on the T1 terrace) age: 19.0 ± 2.0/-2.3 ka; inheritance: 14.48 ± 3.34/-3.43 × 10⁴ atoms/g^c										
WHSL1-1	39.7741°N/74.7324°E	2,560	0	2	26.49	1.00	30.7461	0.3064	96.44 ± 2.17	62.52 ± 1.48
WHSL1-2	39.7741°N/74.7324°E	2,560	30	6	26.49	1.00	30.1013	0.3037	67.36 ± 7.44	44.01 ± 5.00
WHSL1-3	39.7741°N/74.7324°E	2,560	60	4	26.49	1.00	30.0362	0.3015	55.99 ± 1.34	36.29 ± 0.95
WHSL1-4	39.7741°N/74.7324°E	2,560	90	4	26.49	1.00	30.1130	0.2854	49.31 ± 1.43	30.10 ± 0.95
WHSL1-5	39.7741°N/74.7324°E	2,560	120	4	26.49	1.00	28.0963	0.2875	37.80 ± 1.25	24.76 ± 0.91
WHSL1-6	39.7741°N/74.7324°E	2,560	160	4	26.49	1.00	28.7347	0.2748	32.09 ± 1.01	19.54 ± 0.69
WHSL2 (depth sample on the T2b terrace) age: 140.7 ± 15.9/-16.2 ka; inheritance: 11.50 ± 8.09/-10.32 × 10⁴ atoms/g^c										
WHSL2-1	39.7612°N/74.7337°E	2,590	2	4	27.00	1.00	30.4364	0.3190	474.90 ± 8.60	326.48 ± 5.99
WHSL2-2	39.7612°N/74.7337°E	2,590	30	4	27.00	1.00	30.3338	0.2817	411.17 ± 6.75	250.38 ± 4.18
WHSL2-3	39.7612°N/74.7337°E	2,590	55	4	27.00	1.00	30.2053	0.2887	292.31 ± 6.06	183.02 ± 3.87
WHSL2-4	39.7612°N/74.7337°E	2,590	85	4	27.00	1.00	30.3870	0.2895	205.57 ± 5.04	128.11 ± 3.22
WHSL2-5	39.7612°N/74.7337°E	2,590	125	4	27.00	1.00	29.5020	0.2929	123.74 ± 3.10	80.10 ± 2.09
WHSL2-6	39.7612°N/74.7337°E	2,590	160	4	27.00	1.00	30.1918	0.2851	94.11 ± 1.92	57.80 ± 1.25
WHSL2-7	39.7612°N/74.7337°E	2,590	200	6	27.00	1.00	30.3442	0.2933	55.80 ± 1.7	34.82 ± 1.14
WHSL3 (depth sample on the T3b terrace) age: 187.1 ± 34.2/-23.4 ka; inheritance: 9.71 ± 12.14/-8.78 × 10⁴ atoms/g^c										
WHSL3-1	39.7817°N/74.7414°E	2,650	0	2	28.06	1.00	30.4130	0.2956	751.52 ± 10.54	479.49 ± 6.79
WHSL3-2	39.7817°N/74.7414°E	2,650	30	4	28.06	1.00	30.5491	0.3171	435.21 ± 6.57	296.26 ± 4.55
WHSL3-3	39.7817°N/74.7414°E	2,650	65	4	28.06	1.00	30.3817	0.2932	295.41 ± 5.07	186.76 ± 3.28
WHSL3-4	39.7817°N/74.7414°E	2,650	90	4	28.06	1.00	30.4655	0.3096	196.29 ± 5.78	130.45 ± 3.93
WHSL3-5	39.7817°N/74.7414°E	2,650	120	4	28.06	1.00	30.1676	0.2895	136.29 ± 4.04	85.35 ± 2.61

(Continued on the following page)

TABLE 1 (Continued) Analytical results of terrestrial cosmogenic nuclide ¹⁰Be geochronology.

Sample no.	Latitude/Longitude	Elevation (m)	Depth (cm)	Thickness (cm)	Production rate (atoms/g/a) ^a	Shielding correction	Mass qtz (g)	⁹ Be carrier (mg)	¹⁰ Be/ ⁹ Be (10 ⁻¹⁴) ^b	¹⁰ Be concentration (10 ⁴ atoms/g)
WHSL3-6	39.7817°N/74.7414°E	2,650	155	4	28.06	1.00	30.0598	0.3133	94.39 ± 2.13	63.98 ± 1.53
WHSL3-7	39.7817°N/74.7414°E	2,650	200	6	28.06	1.00	30.3100	0.2897	55.81 ± 1.46	34.44 ± 0.98
WHSL4 (surface sample on the T2a terrace) age: 90.4 ± 5.9 ka^d										
WHSL4	39.7856°N/74.7314°E	2,670	2	4	28.42	1.00	30.226	0.2898	428.61 ± 7.01	269.49 ± 4.48
WHSL5 (surface sample on the T4 terrace) age: 160.7 ± 10.4 ka^d										
WHSL5	39.7411°N/74.7550°E	2,510	2	4	25.64	1.00	31.4707	0.2956	674.30 ± 10.08	429.06 ± 6.49

^aProduction rates are from the CRONUS calculator (Balco et al., 2008) and the script of Hidy et al. (2010).

^bAccelerator mass spectrometry measurements used the standard 07KNSTD (¹⁰Be/⁹Be ratio of 2.851 × 10⁻¹²; Nishizumi et al., 2007). Nuclide ratios were corrected using blank samples (a total of three blanks were tested), with an error of 1σ.

^cAge and inheritance of depth profile samples from the Monte Carlo simulation calculator (version 1.2) of Hidy et al. (2010) with 95% upper and lower bounds.

^d¹⁰Be concentrations of surface samples were corrected for inheritance using the depth profiles. Ages were calculated using the LSDn, production rate model (Lifton et al., 2014), with age uncertainties that included both analytical errors and ¹⁰Be production rate errors (sample density of 2.7 g/cm³).

4 Results

4.1 Characteristics of fluvial terrace development

4.1.1 Overall distribution characteristics

The Kaertanv River terraces can be divided approximately into four phases according to their height above the modern riverbed, relative position, and surface weathering (Figures 2–4). East bank terraces are broader and more widespread than those on the west bank. The earliest (T4) terrace is 90–130 m above the present-day riverbed, and occurs solely on the east bank. Weathering and erosion have strongly damaged this terrace surface. Bedrock is widely exposed along this terrace scarp and outer gully, with a 15–36 m-thick gravel layer. North of T4, T3 can be subdivided into T3b and T3a, with deep gullies developed; T3b is 75–100 m above the riverbed and has a >40 m-thick gravel layer, whereas T3a is ~10 m lower. The largest terrace on both river banks is T2, and this can be subdivided into T2a and T2b; T2b is 45–75 m above the riverbed and has a 30–40 m-thick gravel layer, whereas T2a is 5–7 m lower. Terrace 1 is 20–30 m above the riverbed, can be separated into T1a and T1b, and bedrock exposure is only locally visible in the terrace scarp and steep gullies.

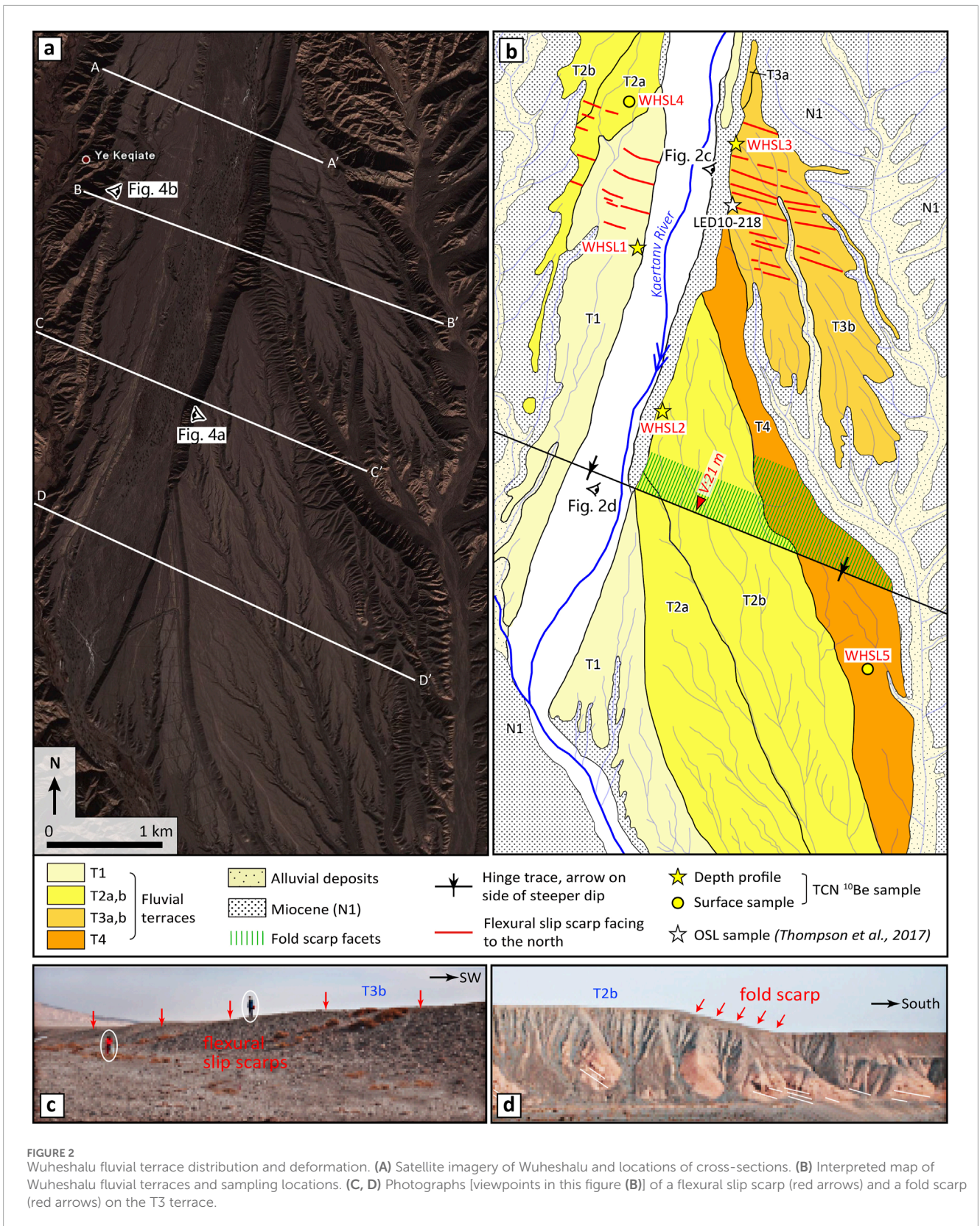
The Wuheshalu terraces are predominantly strath terraces underlain by Miocene dark-red and brownish-red muddy siltstone (Figures 3, 4). The terrace deposits consist of bluish-gray and gray-black fluvial gravel layers, with well-rounded, moderately sorted gravel ranging from approximately 2–10 cm in diameter, with the largest examples exceeding 30 cm. This gravel, which mainly comprises gray-black and bluish-gray metamorphic sandstone with some quartzite and limestone, is clast-supported with a fine to medium-grained sand matrix. The Quaternary deposits in these four terraces exhibit similar sedimentary characteristics.

4.1.2 Cross-sectional distribution characteristics

Fluvial terrace formation varies greatly between river sections. Hence, we conducted a detailed examination of fluvial terrace development and sedimentary structures along four cross-sections from north to south (Figures 3, 4).

The northernmost profile A-A' (Figures 2A, 3A) contains three terraces: T3, T2, and T1, with a riverbed elevation at this point of ~2,600 m. The T3b terrace on the east bank is ~75 m above the present-day riverbed. The terrace deposits feature a ~58 m-thick gravel layer, with a ~40 m-thick finer gravel layer in the upper section and coarser gravel in the lower section. The T2 terrace, developed on the west bank, includes T2b and T2a, which are ~61 and ~53 m above the present-day riverbed, respectively. The T1 terrace, developed on both banks, includes T1b and T1a, which are ~22 and 16–17 m above the present-day riverbed, respectively. Terrace T1a on the east bank exposes Miocene bedrock with a ~13 m-thick gravel layer, while no bedrock exposure is observed in other terraces.

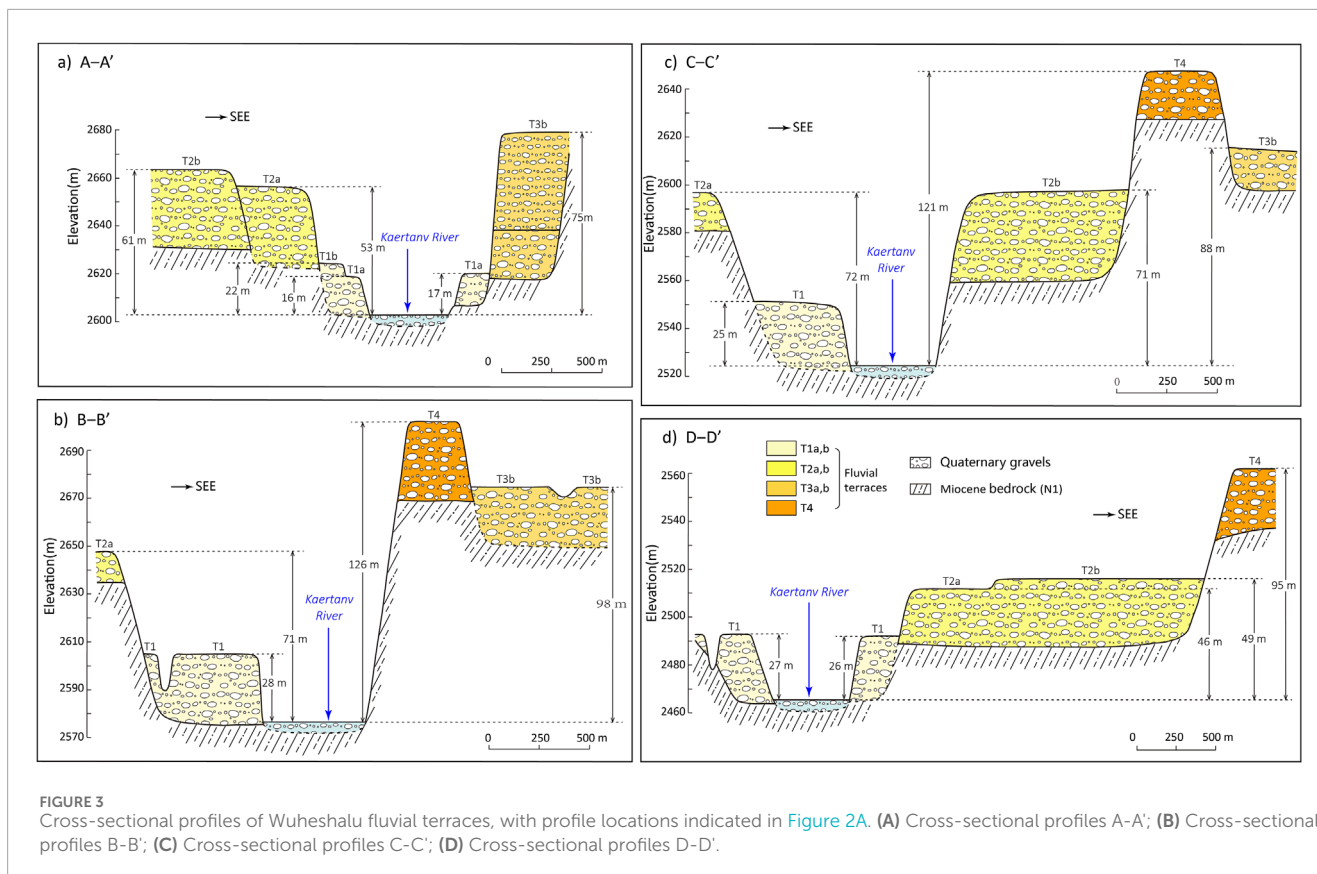
Profile B-B', approximately 1 km south of profile A-A' (Figures 2A, 3B), contains four terraces: T4, T3, T2, and T1, with a present riverbed elevation of ~2,580 m. The T4 and T3b terraces are present on the east bank; T4, which is ~126 m above the present-day



riverbed, has a ~32 m-thick gravel layer on the exposed bedrock; T3b, which is ~98 m above the present-day riverbed, has a gravel layer >25 m in thickness. The T2a and T1 terraces are present on the west bank: T2a, which is ~71 m above the present-day riverbed,

has a ~13 m-thick gravel layer and exposed bedrock, whereas T1 is ~28 m above the present-day riverbed with no bedrock exposure.

Profile C-C', approximately 2 km south of profile B-B' (Figures 2A, 3C), contains four terraces: T4, T3, T2, and T1, and



at this section the current riverbed elevation is $\sim 2,520$ m. The T4 and T3b terraces are present on the east bank: T4, which is ~ 121 m above the present-day riverbed, features a ~ 37 m-thick gravel layer and heavily eroded terrace surface, whereas T3b is ~ 98 m above the present-day riverbed with no bedrock exposure. The T2 terrace includes T2b on the east bank and T2a on the west bank, being ~ 71 and ~ 72 m above the present-day riverbed, with gravel layers of ~ 37 and 13 – 18 m thickness, respectively. The T1 terrace, developed on the west bank, is ~ 25 m above the present-day riverbed with no bedrock exposure.

Profile D-D', approximately 2 km south of profile C-C' (Figures 2A, 3D), contains three terraces: T4, T2, and T1, with a present riverbed elevation of $\sim 2,465$ m. Terrace T4 on the east bank, ~ 95 m above the present-day riverbed, features a 24–36 m-thick gravel layer and heavily eroded terrace surface. Terrace T2 on the east bank includes T2b and T2a, which are ~ 49 and ~ 46 m above the present-day riverbed, respectively. The T1 terrace, 25–26 m above the present-day riverbed, features a ~ 13 m-thick gravel layer and exposed bedrock in deeply incised gullies on the west bank.

4.2 Deformation characteristics of fluvial terraces

The Wuheshalu syncline has undergone substantial deformation since the late Quaternary, affecting the Kaertanv River terraces. In the northern part of the syncline, nearly parallel distribution fault scarps, dipping northwards and perpendicular to the river valley,

have developed owing to bedding-plane slip during fold formation (Figures 2B, C) (Aravind et al., 2022; Li et al., 2013a). The T1a and T3b fault scarp heights are 0.1–0.7 and 0.5–4.3 m, respectively, and they tend to increase with age. Farther south, a SE-striking, ~ 21 m-high and ~ 350 m-wide topographic scarp, with a slope of $\sim 6^\circ$ S, deforms the T2b terrace (Figures 2B, D). This scarp can be traced laterally on the T2b tread and is associated with, and trends parallel to, the southern synclinal hinge in underlying beds. These features support the interpretation of this scarp as a typical fold scarp resulting from hinge migration (Li et al., 2017). Notably, these fault-scarps extend across T3 and T1, whereas the fold-related scarp extends eastwards to the T4 terrace but is not evident on the T1, suggesting a major reduction in fold activity after the T1 terrace formed.

4.3 Age of terraces

Thompson et al. (2017) used OSL dating of fine-grained quartz to date the T3b terrace on the east bank of the Wuheshalu syncline, obtaining an age of 41.3 ± 13.4 ka. The age of T3b obtained using this approach may be overestimated, owing to the common issue of insufficient bleaching in fine-grained quartz (Thompson et al., 2018). Here, ^{10}Be depth profile samples WHSL3, WHSL2, and WHSL1 were collected from the east bank T3b and T2b terraces, and west bank T1 terrace, respectively; ^{10}Be surface samples WHSL5 and WHSL4 were obtained from the east bank T4 terrace and west bank T2a terrace, respectively (Figure 2B). The sample processing

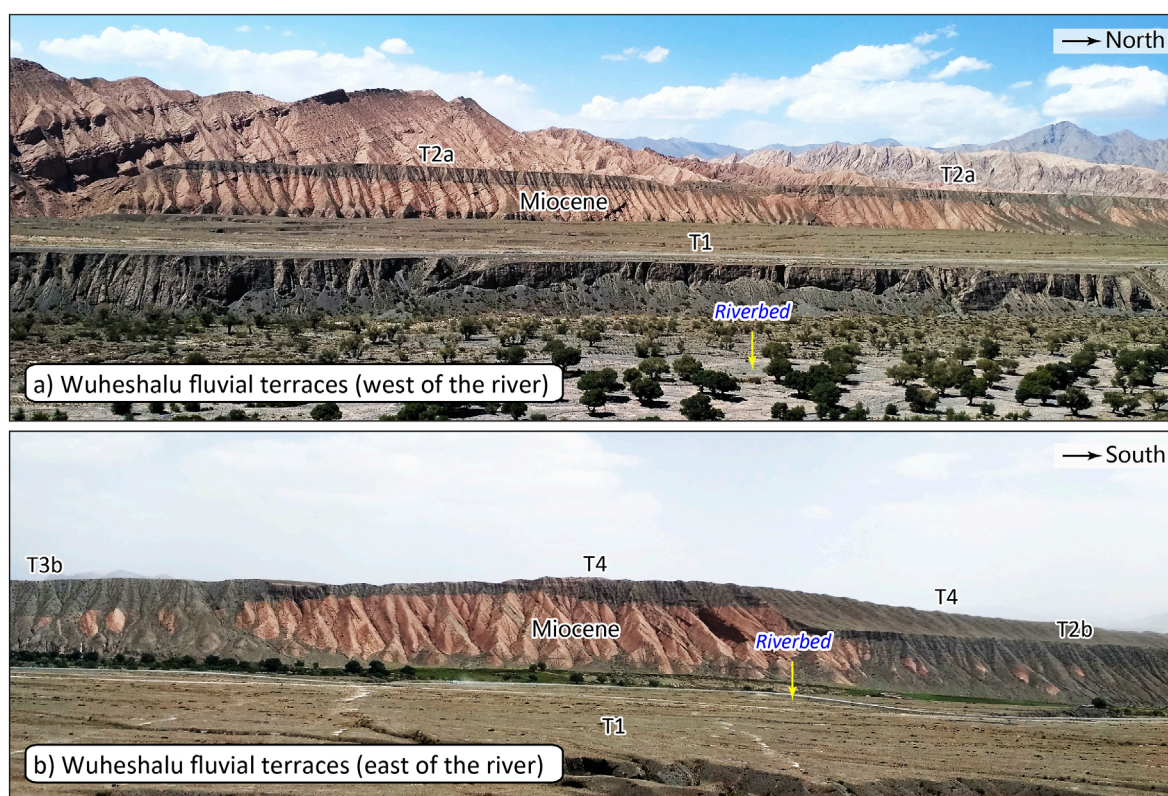


FIGURE 4 Wuheshalu fluvial terraces on the (A) western and (B) eastern banks of the Kaertanv River, with locations of the photographs indicated in Figure 2A.

and testing procedures are detailed in Section 3, and the results are presented in Table 1.

The abandonment ages of terraces T3b, T2b, and T1, obtained from depth profile samples, were $187.1 \pm 34.2/-23.4$, $140.7 \pm 15.9/-16.2$, and $19.0 \pm 2.0/-2.3$ ka, respectively (Figure 5A–C). After correcting the ^{10}Be concentrations of surface samples using the average inheritance from the depth profile samples, the ages of the T4 and T2a terraces were determined to be 160.7 ± 10.4 and 90.4 ± 5.9 ka, respectively. Surface erosion rates were ignored in the calculations. Thus, these data represent the minimum abandonment ages. The dating results apparently indicate that T4, the highest terrace in the region, is younger than T3b; this is likely to be the result of the development of deeply incised gullies and intense weathering erosion on the T4 terrace surface.

Notably, the T3b terrace age obtained here (~ 187 ka) is much older than the ~ 41 ka age obtained using OSL dating (Thompson et al., 2017). Incomplete bleaching of river terrace sediments, mostly fluvial and alluvial gravel deposits, might reduce the accuracy of fine-grained sediment dating techniques such as OSL and ESR dating (Gosse and Phillips, 2001).

The physical mechanism of cosmogenic nuclide dating is well-defined, with relatively few affecting variables, allowing for the direct dating of coarse clastic deposits, such as gravel and coarse sand, to establish geomorphic surface exposure or burial ages. The ^{10}Be depth profile dating results obtained herein are within an acceptable error range, and sample ^{10}Be concentrations from a given depth profile

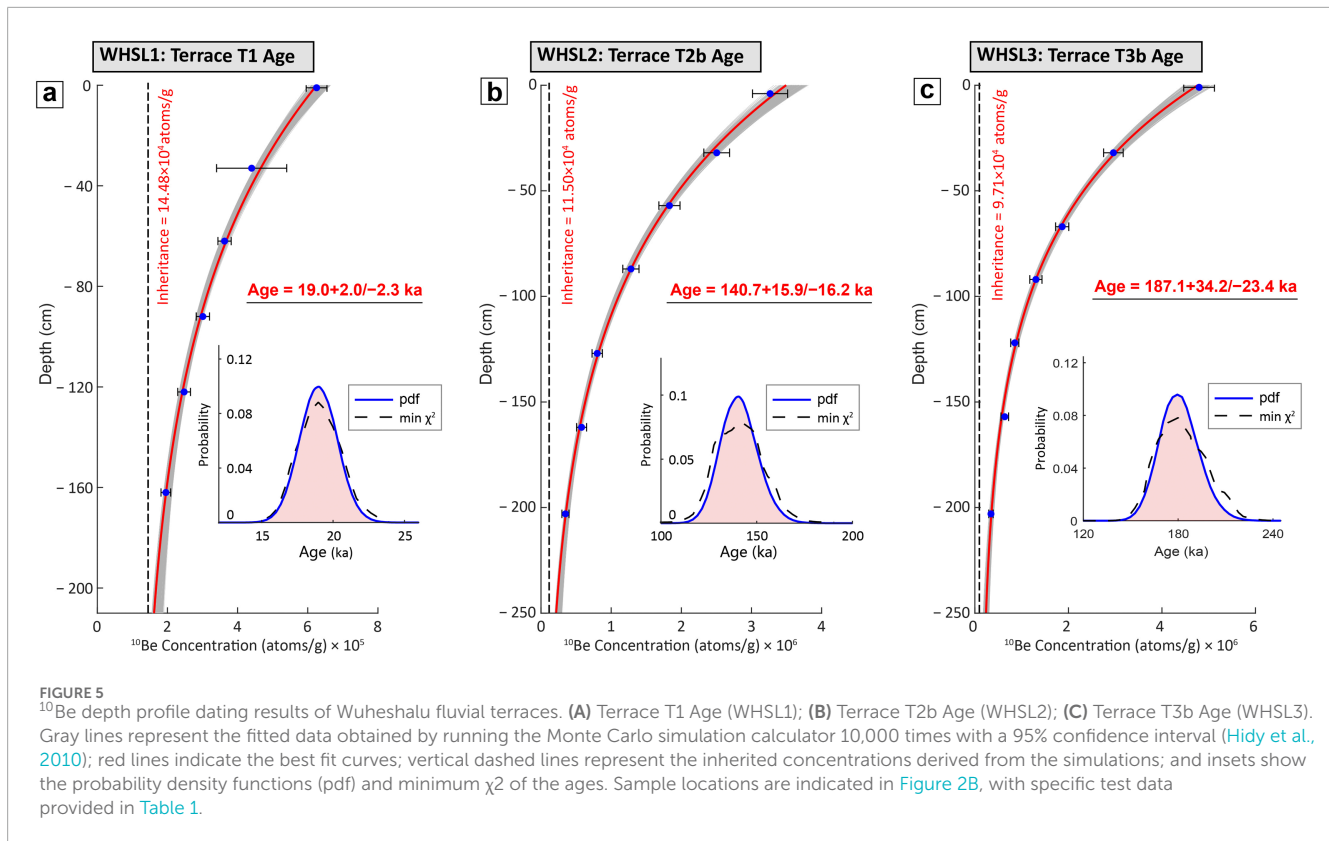
decline exponentially with depth (Figure 5C). Therefore, the T3b age of ~ 187 ka is considered reliable.

5 Discussion

5.1 Relationship between fluvial terrace formation and climate change

Climate change primarily influences river aggradation and incision processes by changing the ratio of sediment flux to water discharge, thereby controlling fluvial terrace development (Bull, 1990; Penck and Brückner, 1909; Scherler et al., 2015; Singh et al., 2024). Numerous studies have demonstrated that fluvial terraces were abandoned during climatic transitions and correspond well with regional climate change (e.g., Bridgland and Westaway, 2008; Cordier et al., 2006; Deschodt et al., 2004; Gao et al., 2016; Hu et al., 2007; Huang et al., 2019; Maddy et al., 2012; Pan et al., 2007; 2013; Starkel, 2003; Stinchcomb et al., 2012; Tao et al., 2020; Thompson et al., 2018). Most terraces were abandoned during climate warming periods, specifically glacial-interglacial transition periods. A small number of terraces have been shown to emerge during cooling periods, such as interglacial-glacial transitions (e.g., Dey et al., 2016; Huang et al., 2014; Schildgen et al., 2016; Strecker et al., 2003; Yang et al., 2020).

We have compared the abandonment ages of Wuheshalu terraces with regional climate proxies and glacial records (Figure 6)



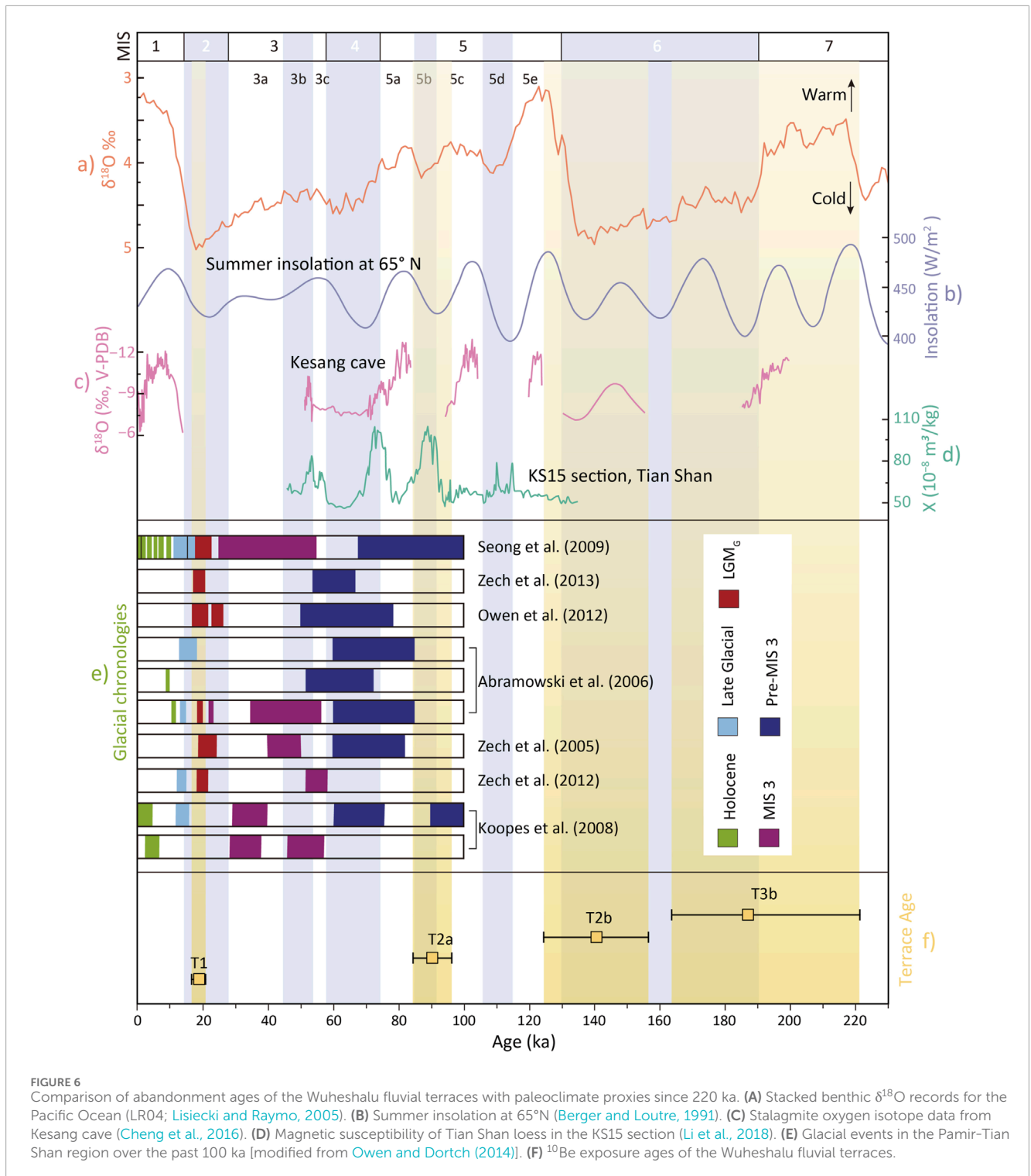
(Abramowski et al., 2006; Koppes et al., 2008; Owen et al., 2012; Seong et al., 2009; Zech, 2012; Zech et al., 2005; Zech et al., 2013). Regional climate proxies used in our comparison include stacked benthic $\delta^{18}\text{O}$ records (LR04; Lisiecki and Raymo, 2005), 65°N summer insolation records (Berger and Loutre, 1991), Kesang Cave stalagmite $\delta^{18}\text{O}$ records (Cheng et al., 2016), and magnetic susceptibility records from the KS15 loess section (Li et al., 2018).

According to our ^{10}Be exposure dating, the T3b, T2b, T2a, and T1 Wuheshalu terraces were abandoned at ~ 187 , ~ 141 , ~ 90 , and ~ 19 ka, respectively. These terrace ages correlate well with regional climate change records (Figure 6). Overall, fluvial incision and terrace formation occurred during glacial-interglacial (MIS6/5, cold-to-warm transition in MIS5, and end of MIS2 or MIS2/1) or interglacial-glacial (MIS7/6) transitions, matching regional climate proxies and glacial records in the Pamir-Tian Shan region.

The T2b terrace formed during the MIS6/5 glacial-interglacial transition period (Lisiecki and Raymo, 2005). During this period, $\delta^{18}\text{O}$ values from Kesang Cave increased from low to high, indicating a gradual rise in precipitation and temperature associated with the westerlies (Cheng et al., 2016). The age of the T2a terrace correlates with the global climate transition from MIS5c to MIS5b (warm to cold; Lisiecki and Raymo, 2005); however, it also corresponds closely to the transition from low to high magnetic susceptibility in the KS15 record (Li et al., 2018) and the large-scale transition from glacial advance to retreat identified in the Tian Shan region during MIS5 (Koppes et al., 2008). Based on the characteristics of regional climate change the T2a terrace also formed during a cold-to-warm transition period, similar to

a glacial-interglacial transition. The T1 terrace formed at the end of MIS2 or during the transition period from MIS2 to MIS1 (Lisiecki and Raymo, 2005). This period matches well with the last major glacial advance (LGM) to glacial retreat (interglacial) in the Pamir-Tian Shan region. According to previous studies (Owen et al., 2012; Zech et al., 2005; 2013), the last significant glacial advance in the Pamir region ended at approximately 17–19 ka, and was followed by glacial retreat. Therefore, the ages of the T2b, T2a, and T1 terraces correspond well with global climate change and glacial advance/retreat records in the Pamir region, with all these terraces forming during glacial-interglacial transition periods. As temperatures rise during a cold-to-warm transition, atmospheric precipitation and meltwater from ice and snow increase, increasing river runoff and transport capacity. Simultaneously, increased vegetation may reduce upstream mountain erosion and sediment flux. Thus, the overall ratio of sediment flux to water discharge decreases, resulting in river downcutting and lateral erosion forming terraces (Maddy et al., 2001). This climatic response pattern of terrace formation during cold (glacial) to warm (interglacial) transitions has been proven in numerous locations, including the Pamir, Southern Tian Shan, and the Shiyang River and Qilianshan Shan. (e.g., Gao et al., 2016; Huang et al., 2019; Pan et al., 2007; Tao et al., 2020; Wu et al., 2018).

Comparative analysis of the T3b terrace age with climatic data indicates that it formed during the MIS7/6 interglacial-glacial transition period (Figure 6; Lisiecki and Raymo, 2005). Summer insolation records and $\delta^{18}\text{O}$ values from Kesang Cave stalagmites also reveal a shift in climate from warm to cold, supporting a widespread glacial advance in the Pamir-Tian Shan region



(penultimate glaciation and/or earlier; Owen et al., 2012; Seong et al., 2009). Fluvial incision versus aggradation depends on the ratio of sediment flux to river discharge (Bull, 1990; Scherler et al., 2015; Singh et al., 2024). Under the condition of decreasing rainfall and an increasingly colder atmosphere, the areal extent of mountain glaciers increased within the Himalaya-Qingzang orogenic belt. However, our results indicate that terrace sediment cycles in the

Pamir-Tian Shan region are predominantly controlled by changes in sediment flux during the MIS7/6 transition period. Thus, during an interglacial-glacial transition period, the ratio of sediment flux to water discharge can also decrease, driving river incision and terrace development (Dey et al., 2016; Scherler et al., 2015). This phenomenon has also been reported from the Qilian Mountains (Yang et al., 2020), Tian Shan (Huang et al., 2014), Pamir Plateau

(Strecker et al., 2003), NW Himalaya (India; Dey et al., 2016), and NW Argentina (Schildgen et al., 2016).

Comparative analysis with terrace dating results from other regions indicates that accurately dated T3b to T1 terraces are widespread in the Pamir–Tian Shan region, showing substantial regional correlation. Molnar et al. (1994) identified a ~180 ka terrace on the Dushanzi anticline in the northern Tian Shan via ^{10}Be dating, which correlates with the T3b terrace identified herein. Fluvial terraces with ages of ~130–145 ka have been recognized associated with the Mushi anticline, Urumqi River, and Yushanguxi River; these are comparable with the T2b terrace identified herein (Li et al., 2013a; Lu et al., 2014; Wu et al., 2018). Terraces with ages similar to the T2a terrace have been reported from the Muji River (~95 ka; Ran, 2009) and Mingyaole anticline (80–82 ka; Wang et al., 2005). The T1 terrace is found throughout the Pamir–Tian Shan region, dated at 16–22 ka, including at locations such as the Mushi anticline and Mayikake Basin in the convergence zone, Manas and Anjihai rivers in the northern Tian Shan, and Yushanguxi River in the southern Tian Shan (Gong et al., 2014; Li et al., 2012; Li et al., 2013a; Thompson et al., 2018; Wang and Wang, 2000; Wu et al., 2018). Regional correlations of terrace ages suggest that fluvial terrace development and incision in the Pamir–Tian Shan region are intimately linked to regional climatic variations, principally influenced by periodic climatic change. Notably, influenced by rapid millennial-scale climatic swings (Bond et al., 2001; Mayewski et al., 2004; Seong et al., 2009), we did not find widely developed Holocene fluvial terraces in the Pamir–Tian Shan region (e.g., Li et al., 2019; Thompson et al., 2018; Wu et al., 2018). Further research is needed to elucidate the specific conditions associated with such terraces.

In summary, the Wuheshalu syncline contains four major fluvial terraces, with the ages of the T3b, T2b, T2a, and T1 terraces being ~187, ~141, ~90, and ~19 ka, respectively. These four fluvial terraces correlate with Pamir–Tian Shan regional climate change and glacial advance/retreat cycles. They were formed during glacial–interglacial (MIS6/5, cold–warm transition of MIS5, and end of MIS2 or MIS2/1) and interglacial–glacial (MIS7/6) climate transitions. This indicates that fluvial incision and terrace development in the Pamir–Tian Shan collision zone are intimately linked to regional periodic variations in climate.

5.2 Relationship between fluvial incision and tectonic uplift

According to the fluvial terrace genesis hypothesis, tectonic uplift primarily provides the driving force and space for river incision. In tectonically stable areas, owing to limited incision space, periodic climatic fluctuations often result in the formation of nested aggregational terraces. Only in regions with at least moderate tectonic uplift rates, where sufficient space is provided for river downcutting, are rhythmic climatic fluctuations particularly suitable for the formation of river terraces (Bridgland and Allen, 1996; Bridgland et al., 2004; Maddy et al., 2001; Maddy et al., 2012; Pan et al., 2003; Pan et al., 2009; Starkel, 2003; Vandenbergh and Maddy, 2001).

Fluvial incision rates across different periods can be calculated by integrating terrace elevation above the modern riverbed, height variations between terraces, and abandonment ages (Palamakumbura et al., 2016). Along the northern scarp profile

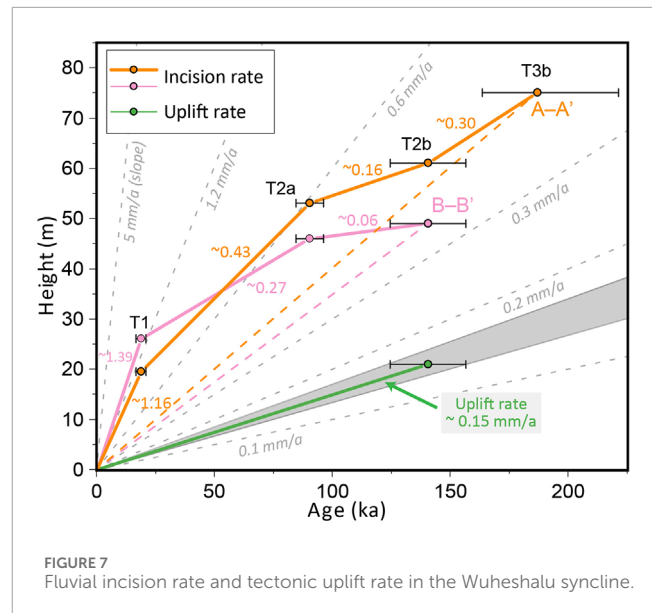


FIGURE 7
Fluvial incision rate and tectonic uplift rate in the Wuheshalu syncline.

A–A', terrace T3b is ~75 m above the modern riverbed, and the terrace riser heights of T3b/T2b, T2b/T2a, T2a/T1, and T1/T0 are ~14, ~8, ~31, and ~22 m, respectively. On the basis of the dating results of each terrace, the average incision rate has been ~0.40 mm/a since the formation of terrace T3b at ~187.1 ka. Specifically, the incision rate between T3b and T2b (~140.7 ka) was ~0.30 mm/a, and that between T2b and T1 (~19.0 ka) was 0.16–0.43 mm/a; since the formation of the T1 terrace, the incision rate has increased to ~1.16 mm/a (Figure 7). Thus, the Kaertanv River has had an unstable incision rate since the Pleistocene. Along the southern scarp profile D–D', terraces T2b, T2a, and T1 are ~49, ~46, and ~25 m above the modern riverbed. The average incision rate has been ~0.35 mm/a since the formation of the T2b terrace. Between terraces T2b and T1, the incision rate was ~0.06–0.27 mm/a; after the formation of T1, it rose to ~1.39 mm/a (Figure 7). In summary, these results indicate that the magnitudes and trends of river incision rates on both sides of the fold scarp have been highly consistent, whereas tectonic uplift has had a minimal impact.

A series of fault and fold scarps have formed on the terrace surfaces owing to extensive tectonic deformation (Figure 2B). The fold scarp of the T2b was measured to be 21 m height using differential GPS topographic measurements (Li et al., 2017). This height is considered to represent the net vertical uplift of T2b (Figures 2B, D). The abandonment ages of terraces T2b are determined to be 140.7 +15.9/–16.2 ka in this study. The vertical offset and age of the terrace yield a tectonic uplift rate of ~0.15 mm/a since its development (Figure 7). Compared with the fluvial incision rate on the elevated side of the fold, tectonic uplift accounts for only one-third of the total incision rate. In summary, tectonic uplift appears to only minimally affect fluvial incision; instead, regional climatic variations or glacial/interglacial aggradation/incision processes appear to regulate fluvial incision in the Pamir–Tian Shan collision zone. Our finding that the fluvial incision rate is markedly higher than the tectonic uplift rate is consistent with the results of studies in

the northern Tian Shan and Qilian Mountains (Gong et al., 2014; Hu et al., 2020; Yang et al., 2020).

6 Conclusion

In this study, we have established the geomorphological sequence and chronological framework of the Wuheshalu terraces through geomorphological interpretation, field investigation, and TCN ¹⁰Be depth profile and surface gravel exposure dating. Four major fluvial terraces (T4, T3a/b, T2a/b, and T1) were identified in the Wuheshalu syncline, most of which are bedrock-seated terraces. The ages of the T3b, T2b, T2a, and T1 terraces are approximately 187, 141, 90, and 19 ka, respectively. These four terraces correspond well with regional changes in climate and glacial advance or retreat events in the Pamir–Tian Shan region, forming during glacial–interglacial (MIS6/5, cold-to-warm transition period of MIS5, and end of MIS2 or MIS2/1) and interglacial–glacial (MIS7/6) climatic transitions. Analysis of fluvial incision and tectonic uplift rates indicates that tectonic uplift-induced fluvial incision in the Wuheshalu syncline accounts for only one-third of the total incision rate. These results suggest that fluvial incision and terrace formation in the Pamir–Tian Shan collision zone are likely driven by periodic climatic fluctuations, in particular glacial advance- or retreat-controlled aggradation/incision processes, with tectonic uplift providing only a minimal contribution.

Data availability statement

The original contributions presented in the study are included in the article/supplementary material, further inquiries can be directed to the corresponding author.

Author contributions

JD: Data curation, Formal Analysis, Investigation, Methodology, Writing–original draft, Writing–review and editing, Conceptualization. TL: Conceptualization, Funding acquisition,

Supervision, Writing–review and editing, Formal Analysis, Visualization. JF: Formal Analysis, Visualization, Writing–review and editing. LQ: Formal Analysis, Methodology, Project administration, Writing–review and editing.

Funding

The author(s) declare that financial support was received for the research, authorship, and/or publication of this article. This study was funded by the Key R&D Program of Xinjiang Uygur Autonomous Region (No. 2022B03001-1) and Institute of Geology, China Earthquake Administration (No. IGCEA1920).

Acknowledgments

We gratefully thank the reviewers and the editor for their valuable comments and suggestions on the manuscript.

Conflict of interest

Author JD was employed by Sichuan Institute of Geological Engineering Investigation Group Co., Ltd. Author JF was employed by China Academy of Railway Sciences Co., Ltd.

The remaining authors declare that the research was conducted in the absence of any commercial or financial relationships that could be construed as a potential conflict of interest.

Publisher's note

All claims expressed in this article are solely those of the authors and do not necessarily represent those of their affiliated organizations, or those of the publisher, the editors and the reviewers. Any product that may be evaluated in this article, or claim that may be made by its manufacturer, is not guaranteed or endorsed by the publisher.

References

- Abramowski, U., Bergau, A., Seebach, D., Zech, R., Glaser, B., Sosin, P., et al. (2006). Pleistocene glaciations of Central Asia: results from 10Be surface exposure ages of erratic boulders from the Pamir (Tajikistan), and the Alay–Turkestan range (Kyrgyzstan). *Quat. Sci. Rev.* 25 (9–10), 1080–1096. doi:10.1016/j.quascirev.2005.10.003
- Aravind, A., Mishra, R. L., Jagtap, S., Jayangondaperumal, R., Thakur, V. C., Pant, C. C., et al. (2022). Detachment folding, growth mechanism and seismic potential in the Jammu Sub-Himalaya. *J. Struct. Geol.* 155, 104514. doi:10.1016/j.jsg.2022.104514
- Balco, G., Stone, J. O., Lifton, N. A., and Dunai, T. J. (2008). A complete and easily accessible means of calculating surface exposure ages or erosion rates from 10Be and 26Al measurements. *Quat. Geochronol.* 3 (3), 174–195. doi:10.1016/j.quageo.2007.12.001
- Berger, A., and Loutre, M.-F. (1991). Insolation values for the climate of the last 10 million years. *Quat. Sci. Rev.* 10 (4), 297–317. doi:10.1016/0277-3791(91)90033-q
- Bond, G., Kromer, B., Beer, J., Muscheler, R., Evans, M. N., Showers, W., et al. (2001). Persistent solar influence on north atlantic climate during the Holocene. *Science* 294 (5549), 2130–2136. doi:10.1126/science.1065680
- Bridgland, D., and Allen, P. (1996). “A revised model for terrace formation and its significance for the lower Middle Pleistocene Thames terrace aggradations of south-east Essex,” in *The early middle Pleistocene in Europe* (Rotterdam: Balkema), 123–134.
- Bridgland, D., Maddy, D., and Bates, M. (2004). River terrace sequences: templates for Quaternary geochronology and marine–terrestrial correlation. *J. Quat. Sci.* 19 (2), 203–218. doi:10.1002/jqs.819
- Bridgland, D., and Westaway, R. (2008). Climatically controlled river terrace staircases: a worldwide Quaternary phenomenon. *Geomorphology* 98 (3–4), 285–315. doi:10.1016/j.geomorph.2006.12.032
- Bull, W. B. (1990). Stream-terrace genesis: implications for soil development. *Geomorphology* 3 (3–4), 351–367. doi:10.1016/0169-555x(90)90011-e
- Burtman, V. S., and Molnar, P. (1993). *Geological and geophysical evidence for deep subduction of continental crust beneath the Pamir*. Boulder, Colorado: Geological Society of America. Special Paper 281.
- Carroll, A., Graham, S., Hendrix, M., Ying, D., and Zhou, D. (1995). Late Paleozoic tectonic amalgamation of northwestern China: sedimentary record of the northern

- Tarim, northwestern Turpan, and southern Junggar basins. *Geol. Soc. Am. Bull.* 107 (5), 571–594. doi:10.1130/0016-7606(1995)107<0571:lptaon>2.3.co;2
- Chapman, J. B., Carrapa, B., Ballato, P., DeCelles, P. G., Worthington, J., Oimahmadov, I., et al. (2017). Intracontinental subduction beneath the Pamir Mountains: constraints from thermokinematic modeling of shortening in the Tajik fold-and-thrust belt. *Bulletin* 129 (11–12), 1450–1471. doi:10.1130/B31730.1
- Charvet, J., Shu, L., Laurent-Charvet, S., Wang, B., Faure, M., Cluzel, D., et al. (2011). Palaeozoic tectonic evolution of the Tianshan belt, NW China. *Sci. China Earth Sci.* 54, 166–184. doi:10.1007/s11430-010-4138-1
- Chen, F., Yu, Z., Yang, M., Ito, E., Wang, S., Madsen, D. B., et al. (2008). Holocene moisture evolution in arid central Asia and its out-of-phase relationship with Asian monsoon history. *Quat. Sci. Rev.* 27 (3–4), 351–364. doi:10.1016/j.quascirev.2007.10.017
- Chen, J., Li, T., Li, W., and Yuan, Z. (2011). Late cenozoic and present tectonic deformation in the Pamir salient, northwestern China (in Chinese). *Seismol. Geol.* 33 (2), 241–259. doi:10.3969/j.issn.0253-4967.2011.02.001
- Cheng, H., Spötl, C., Breitenbach, S. F., Sinha, A., Wassenburg, J. A., Jochum, K. P., et al. (2016). Climate variations of Central Asia on orbital to millennial timescales. *Sci. Rep.* 6 (1), 36975. doi:10.1038/srep36975
- Cordier, S., Harmand, D., Frechen, M., and Beiner, M. (2006). Fluvial system response to middle and upper pleistocene climate change in the meurthe and moselle valleys (eastern Paris basin and rhenish massif). *Quat. Sci. Rev.* 25 (13–14), 1460–1474. doi:10.1016/j.quascirev.2005.11.007
- Cowgill, E. (2010). Cenozoic right-slip faulting along the eastern margin of the Pamir salient, northwestern China. *Bulletin* 122 (1–2), 145–161. doi:10.1130/b26520.1
- Darling, A. L., Karlstrom, K. E., Granger, D. E., Aslan, A., Kirby, E., Ouimet, W. B., et al. (2012). New incision rates along the Colorado River system based on cosmogenic burial dating of terraces: implications for regional controls on Quaternary incision. *Geosphere* 8 (5), 1020–1041. doi:10.1130/gso0724.1
- Deschodt, L., Salvador, P. G., and Boulou, M. (2004). Sedimentary formations and evolution of the Deule valley since the upper pleniglacial at Houplin-Ancoisne (Northern France). *Quaternaire* 15 (3), 269–284. doi:10.3406/quate.2004.1774
- Dey, S., Thiede, R. C., Schildgen, T. F., Wittmann, H., Bookhagen, B., Scherler, D., et al. (2016). Climate-driven sediment aggradation and incision since the late Pleistocene in the NW Himalaya, India. *Earth Planet. Sci. Lett.* 449, 321–331. doi:10.1016/j.epsl.2016.05.050
- Dumitru, T. A., Zhou, D., Chang, E. Z., Graham, S. A., Hendrix, M. S., Sobel, E. R., et al. (2001). Uplift, exhumation, and deformation in the Chinese Tian Shan. *Geological Society of America Memoirs*, 194, 71–99. doi:10.1130/0-8137-1194-0-71
- Gao, H., Li, Z., Pan, B., Liu, F., and Liu, X. (2016). Fluvial responses to late Quaternary climate change in the Shiyang River drainage system, western China. *Geomorphology* 258, 82–94. doi:10.1016/j.geomorph.2016.01.018
- Gong, Z., Li, S.-H., and Li, B. (2014). The evolution of a terrace sequence along the Manas River in the northern foreland basin of Tian Shan, China, as inferred from optical dating. *Geomorphology* 213, 201–212. doi:10.1016/j.geomorph.2014.01.009
- Gosse, J. C., and Phillips, F. M. (2001). Terrestrial *in situ* cosmogenic nuclides: theory and application. *Quat. Sci. Rev.* 20 (14), 1475–1560. doi:10.1016/s0277-3791(00)00171-2
- Harkins, N., Kirby, E., Heimsath, A., Robinson, R., and Reiser, U. (2007). Transient fluvial incision in the headwaters of the Yellow River, northeastern Tibet, China. *J. Geophys. Res. Earth Surf.* 112 (F3). doi:10.1029/2006jf000570
- Heermance, R. V., Chen, J., Burbank, D. W., and Miao, J. (2008). Temporal constraints and pulsed Late Cenozoic deformation during the structural disruption of the active Kashi foreland, northwest China. *Tectonics* 27 (6). doi:10.1029/2007tc002226
- Hendrix, M. S., Graham, S. A., Carroll, A. R., Sobel, E. R., McKnight, C. L., Schulein, B. J., et al. (1992). Sedimentary record and climatic implications of recurrent deformation in the Tian Shan: evidence from Mesozoic strata of the north Tarim, south Junggar, and Turpan basins, northwest China. *Geol. Soc. Am. Bull.* 104 (1), 53–79. doi:10.1130/0016-7606(1992)104<0053:sracio>2.3.co;2
- Hidy, A. J., Gosse, J. C., Pederson, J. L., Mattern, J. P., and Finkel, R. C. (2010). A geologically constrained Monte Carlo approach to modeling exposure ages from profiles of cosmogenic nuclides: an example from Lees Ferry, Arizona. *Geochem. Geophys. Geosystems* 11 (9). doi:10.1029/2010gc003084
- Hu, G., Chen, J., Qin, J., and Li, S. (2020). Rapid incision events since 3.7 ka in the Anjihaihe Gorge along the northern Tianshan range, China. *Chin. Sci.* 65 (15), 1506–1518. doi:10.1360/tb-2019-0385
- Hu, X., Pan, B., Su, H., An, C., and Chou, T. (2007). Terrace formation age and river incision mechanism of wanchuan river (in Chinese). *Sci. Geogr. Sin.* 27 (6), 808–813. doi:10.13249/j.cnki.sgs.2007.06.808
- Huang, W., Yang, X., Jobe, J. A. T., Li, S., Yang, H., and Zhang, L. (2019). Alluvial plains formation in response to 100-ka glacial-interglacial cycles since the Middle Pleistocene in the southern Tian Shan, NW China. *Geomorphology* 341, 86–101. doi:10.1016/j.geomorph.2019.05.013
- Huang, W.-l., Yang, X.-p., Li, A., Thompson, J. A., and Zhang, L. (2014). Climatically controlled formation of river terraces in a tectonically active region along the southern piedmont of the Tian Shan, NW China. *Geomorphology* 220, 15–29. doi:10.1016/j.geomorph.2014.05.024
- Jay, C. N., Flesch, L. M., and Bendick, R. O. (2017). Kinematics and dynamics of the Pamir, Central Asia: quantifying surface deformation and force balance in an intracontinental subduction zone. *J. Geophys. Res. Solid Earth* 122 (6), 4741–4762. doi:10.1002/2017jb014177
- Jayangondaperumal, R., Thakur, V. C., Vivek, J., Rao, P. S., and Gupta, A. K. (2018). Active tectonics of kumaun and garhwal Himalaya. *Springer Nat. Hazards*, 150. doi:10.1007/978-981-10-8243-6
- Koppes, M., Gillespie, A. R., Burke, R. M., Thompson, S. C., and Stone, J. (2008). Late quaternary glaciation in the Kyrgyz tien Shan. *Quat. Sci. Rev.* 27 (7–8), 846–866. doi:10.1016/j.quascirev.2008.01.009
- Lal, D. (1991). Cosmic ray labeling of erosion surfaces: *in situ* nuclide production rates and erosion models. *Earth Planet. Sci. Lett.* 104 (2–4), 424–439. doi:10.1016/0012-821x(91)90220-c
- Lavé, J., and Avouac, J.-P. (2001). Fluvial incision and tectonic uplift across the Himalayas of central Nepal. *J. Geophys. Res. Solid Earth* 106 (B11), 26561–26591. doi:10.1029/2001jb000359
- Li, G., Chen, F., Xia, D., Yang, H., Zhang, X., Madsen, D., et al. (2018). A Tianshan Mountains loess-paleosol sequence indicates anti-phase climatic variations in arid central Asia and in East Asia. *Earth Planet. Sci. Lett.* 494, 153–163. doi:10.1016/j.epsl.2018.04.052
- Li, T., Chen, J., Thompson, J. A., Burbank, D. W., and Xiao, W. (2012). Equivalency of geologic and geodetic rates in contractional orogens: new insights from the Pamir Frontal Thrust. *Geophys. Res. Lett.* 39 (15). doi:10.1029/2012gl015782
- Li, T., Chen, J., Thompson, J. A., Burbank, D. W., and Yang, H. (2015). Hinge-migrated fold-scarp model based on an analysis of bed geometry: a study from the Mingyale anticline, southern foreland of Chinese Tian Shan. *J. Geophys. Res. Solid Earth* 120 (9), 6592–6613. doi:10.1002/2015jb012102
- Li, T., Chen, J., Thompson, J. A., Burbank, D. W., and Yang, X. (2013a). Quantification of three-dimensional folding using fluvial terraces: a case study from the Mushi anticline, northern margin of the Chinese Pamir. *J. Geophys. Res. Solid Earth* 118 (8), 4628–4647. doi:10.1002/jgrb.50316
- Li, T., Chen, J., Thompson, J. A., and Burbank, D. W. (2017). Active flexural-slip faulting: controls exerted by stratigraphy, geometry, and fold kinematics. *J. Geophys. Res. Solid Earth* 122 (10), 8538–8565. doi:10.1002/2017jb013966
- Li, T., Chen, J., and Xiao, W. (2013b). Late-Quaternary folding of the Mingyale anticline southwestern tip, Pamir-Tianshan convergent zone (in Chinese). *Seismol. Geol.* 35 (2), 234–246. doi:10.3969/j.issn.0253-4967.2013.02.004
- Li, T., Schoenbohm, L. M., Chen, J., Yuan, Z., Feng, W., Li, W., et al. (2019). Cumulative and coseismic (during the 2016 Mw 6.6 Aketao earthquake) deformation of the dextral-slip Muji Fault, northeastern Pamir orogen. *Tectonics* 38 (11), 3975–3989. doi:10.1029/2019tc005680
- Lifton, N., Sato, T., and Dunai, T. J. (2014). Scaling *in situ* cosmogenic nuclide production rates using analytical approximations to atmospheric cosmic-ray fluxes. *Earth Planet. Sci. Lett.* 386, 149–160. doi:10.1016/j.epsl.2013.10.052
- Lisiecki, L., and Raymo, M. (2005). A Pliocene-Pleistocene stack of 57 globally distributed benthic $\delta^{18}\text{O}$ records. *Paleoceanography* 20 (1). doi:10.1029/2004pa001071
- Lu, H., Zhang, T., Zhao, J., Si, S., Wang, H., Chen, S., et al. (2014). Late Quaternary alluvial sequence and uplift-driven incision of the Urumqi River in the north front of the Tian Shan, northwestern China. *Geomorphology* 219, 141–151. doi:10.1016/j.geomorph.2014.05.001
- Maddy, D., Bridgland, D., and Westaway, R. (2001). Uplift-driven valley incision and climate-controlled river terrace development in the Thames Valley, UK. *Quat. Int.* 79 (1), 23–36. doi:10.1016/s1040-6182(00)00120-8
- Maddy, D., Demir, T., Veldkamp, A., Bridgland, D. R., Stemerink, C., Van der Schriek, T., et al. (2012). The obliquity-controlled early Pleistocene terrace sequence of the Gediz River, western Turkey: a revised correlation and chronology. *J. Geol. Soc.* 169 (1), 67–82. doi:10.1144/0016-76492011-011
- Mayewski, P. A., Meeker, L. D., Twickler, M. S., Whitlow, S., Yang, Q., Lyons, W. B., et al. (1997). Major features and forcing of high-latitude northern hemisphere atmospheric circulation using a 110,000-year-long glaciochemical series. *J. Geophys. Res. Oceans* 102 (C12), 26345–26366. doi:10.1029/96jc03365
- Mayewski, P. A., Rohling, E. E., Stager, J. C., Karlén, W., Maasch, K. A., Meeker, L. D., et al. (2004). Holocene climate variability. *Quat. Res.* 62 (3), 243–255. doi:10.1016/j.yqres.2004.07.001
- Molnar, P., Brown, E. T., Burchfiel, B. C., Deng, Q., Feng, X., Li, J., et al. (1994). Quaternary climate change and the formation of river terraces across growing anticlines on the north flank of the Tien Shan, China. *J. Geol.* 102 (5), 583–602. doi:10.1086/629700
- Molnar, P., and Tapponnier, P. (1975). Cenozoic Tectonics of Asia: effects of a Continental Collision: features of recent continental tectonics in Asia can be interpreted as results of the India-Eurasia collision. *science* 189 (4201), 419–426. doi:10.1126/science.189.4201.419
- Nishiizumi, K., Imamura, M., Caffee, M. W., Southon, J. R., Finkel, R. C., and McAninch, J. (2007). Absolute calibration of ^{10}Be AMS standards. *Nucl.*

- Instrum. Methods Phys. Res. Sect. B Beam Interact. Mater. Atoms 258 (2), 403–413. doi:10.1016/j.nimb.2007.01.297
- Owen, L. A., Chen, J., Hedrick, K. A., Caffee, M. W., Robinson, A. C., Schoenbohm, L. M., et al. (2012). Quaternary glaciation of the tashkurgan valley, southeast Pamir. *Quat. Sci. Rev.* 47, 56–72. doi:10.1016/j.quascirev.2012.04.027
- Owen, L. A., and Dortch, J. M. (2014). Nature and timing of Quaternary glaciation in the Himalayan–Tibetan orogen. *Quat. Sci. Rev.* 88, 14–54. doi:10.1016/j.quascirev.2013.11.016
- Palamakumbura, R. N., Robertson, A. H., Kinnaird, T. C., van Calsteren, P., Kroon, D., and Tait, J. A. (2016). Quantitative dating of Pleistocene deposits of the Kyrenia Range, northern Cyprus: implications for timing, rates of uplift and driving mechanisms. *J. Geol. Soc.* 173 (6), 933–948. doi:10.1144/jgs2015-130
- Pan, B., Burbank, D., Wang, Y., Wu, G., Li, J., and Guan, Q. (2003). A 900 ky record of strath terrace formation during glacial–interglacial transitions in northwest China. *Geology* 31 (11), 957–960. doi:10.1130/g19685.1
- Pan, B., Hu, X., Gao, H., Hu, Z., Cao, B., Geng, H., et al. (2013). Late Quaternary river incision rates and rock uplift pattern of the eastern Qilian Shan Mountain, China. *Geomorphology* 184, 84–97. doi:10.1016/j.geomorph.2012.11.020
- Pan, B., Su, H., Hu, Z., Hu, X., Gao, H., Li, J., et al. (2009). Evaluating the role of climate and tectonics during non-steady incision of the Yellow River: evidence from a 1.24 Ma terrace record near Lanzhou, China. *Quat. Sci. Rev.* 28 (27–28), 3281–3290. doi:10.1016/j.quascirev.2009.09.003
- Pan, B., Su, H., Liu, X., Hu, X., Zhou, T., Hu, C., et al. (2007). River terraces of the yellow river and their genesis in eastern Lanzhou basin during last 1.2 Ma (in Chinese). *Quat. Sci.* 27 (2), 172–180. doi:10.3321/j.issn:1001-7410.2007.02.002
- Pan, B., Wu, G., Wang, Y., Liu, Z., and Guan, Q. (2001). Age and genesis of the shagou River terraces in eastern qilian mountains. *Chin. Sci. Bull.* 46, 509–513. doi:10.1007/bf03187270
- Penck, A., and Brückner, E. (1909). *Die Alpen im Eiszeitalter*. Leipzig: Tauchnitz.
- Perrineau, A., Woerd, J. V. D., Gaudemer, Y., Liu-Zeng, J., Pik, R., Tapponnier, P., et al. (2011). Incision rate of the Yellow River in Northeastern Tibet constrained by 10Be and 26Al cosmogenic isotope dating of fluvial terraces: implications for catchment evolution and plateau building. *Geol. Soc. Lond. Spec. Publ.* 353 (1), 189–219. doi:10.1144/sp353.10
- Ran, Z. (2009). *The study of river terraces in the Bulunkou area (in Chinese)* Master. Henan Polytechnic University.
- Robinson, A. C., Yin, A., Manning, C. E., Harrison, T. M., Zhang, S.-H., and Wang, X.-F. (2004). Tectonic evolution of the northeastern Pamir: constraints from the northern portion of the Cenozoic Kongur Shan extensional system, western China. *Geol. Soc. Am. Bull.* 116 (7–8), 953–973. doi:10.1130/b25375.1
- Scharer, K., Burbank, D., Chen, J., Weldon, R., Rubin, C., Zhao, R., et al. (2004). Detachment folding in the Southwestern Tian Shan–Tarim foreland, China: shortening estimates and rates. *J. Struct. Geol.* 26 (11), 2119–2137. doi:10.1016/j.jsg.2004.02.016
- Scherler, D., Bookhagen, B., Wulf, H., Preusser, F., and Strecker, M. R. (2015). Increased late Pleistocene erosion rates during fluvial aggradation in the Garhwal Himalaya, northern India. *Earth Planet. Sci. Lett.* 428, 255–266. doi:10.1016/j.epsl.2015.06.034
- Schildgen, T. F., Robinson, R. A., Savi, S., Phillips, W. M., Spencer, J. Q., Bookhagen, B., et al. (2016). Landscape response to late Pleistocene climate change in NW Argentina: sediment flux modulated by basin geometry and connectivity. *J. Geophys. Res. Earth Surf.* 121 (2), 392–414. doi:10.1002/2015jf003607
- Schurr, B., Ratschbacher, L., Sippl, C., Gloaguen, R., Yuan, X., and Mechie, J. (2014). Seismotectonics of the Pamir. *Tectonics* 33 (8), 1501–1518. doi:10.1002/2014tc003576
- Seong, Y. B., Owen, L. A., Yi, C., and Finkel, R. C. (2009). Quaternary glaciation of muztag Ata and Kongur Shan: evidence for glacier response to rapid climate changes throughout the late glacial and Holocene in westernmost Tibet. *Geol. Soc. Am. Bull.* 121 (3–4), 348–365. doi:10.1130/b26339.1
- Singh, I., Jayagondaperumal, R., Pandey, A., Priyanka, R. S., Mishra, R. L., Morthekai, P., et al. (2024). Late Quaternary deformation, strain partitioning, and fold-thrust belt widening in the Eastern Himalayan Syntaxis, India. *Tectonophysics* 871, 230193. doi:10.1016/j.tecto.2023.230193
- Sobel, E. R., Chen, J., and Heermance, R. V. (2006). Late oligocene–early Miocene initiation of shortening in the southwestern Chinese tian Shan: implications for neogene shortening rate variations. *Earth Planet. Sci. Lett.* 247 (1–2), 70–81. doi:10.1016/j.epsl.2006.03.048
- Sobel, E. R., Schoenbohm, L. M., Chen, J., Thiede, R., Stockli, D. F., Sudo, M., et al. (2011). Late miocene–pliocene deceleration of dextral slip between Pamir and Tarim: implications for Pamir orogenesis. *Earth Planet. Sci. Lett.* 304 (3–4), 369–378. doi:10.1016/j.epsl.2011.02.012
- Starkel, L. (2003). Climatically controlled terraces in uplifting mountain areas. *Quat. Sci. Rev.* 22 (20), 2189–2198. doi:10.1016/s0277-3791(03)00148-3
- Stinchcomb, G. E., Driese, S. G., Nordt, L. C., and Allen, P. M. (2012). A mid to late Holocene history of floodplain and terrace reworking along the middle Delaware River valley, USA. *Geomorphology* 169, 123–141. doi:10.1016/j.geomorph.2012.04.018
- Strecker, M. R., Hilley, G. E., Arrowsmith, J. R., and Coutand, I. (2003). Differential structural and geomorphic mountain-front evolution in an active continental collision zone: the northwest Pamir, southern Kyrgyzstan. *Geol. Soc. Am. Bull.* 115 (2), 166–181. doi:10.1130/0016-7606(2003)115<0166:dsagmf>2.0.co;2
- Tao, Y., Xiong, J., Zhang, H., Chang, H., and Li, L. (2020). Climate-driven formation of fluvial terraces across the Tibetan Plateau since 200 ka: a review. *Quat. Sci. Rev.* 237, 106303. doi:10.1016/j.quascirev.2020.106303
- Thiede, R. C., Sobel, E. R., Chen, J., Schoenbohm, L. M., Stockli, D. F., Sudo, M., et al. (2013). Late Cenozoic extension and crustal doming in the India–Eurasia collision zone: new thermochronologic constraints from the NE Chinese Pamir. *Tectonics* 32 (3), 763–779. doi:10.1002/tect.20050
- Thompson, J., Jessica, A., Li, T., Chen, J., Burbank, D. W., and Bufo, A. (2017). Quaternary tectonic evolution of the Pamir–Tian Shan convergence zone, Northwest China. *Tectonics* 36 (12), 2748–2776. doi:10.1002/2017tc004541
- Thompson, J. A., Chen, J., Yang, H., Li, T., Bookhagen, B., and Burbank, D. (2018). Coarse-versus fine-grain quartz OSL and cosmogenic 10Be dating of deformed fluvial terraces on the northeast Pamir margin, northwest China. *Quat. Geochronol.* 46, 1–15. doi:10.1016/j.quageo.2018.01.002
- Vandenbergh, J., and Maddy, D. (2001). The response of river systems to climate change. *Quat. Int.* 79, 1–3. doi:10.1016/s1040-6182(00)00118-x
- Veldkamp, A., and Van Dijke, J. (2000). Simulating internal and external controls on fluvial terrace stratigraphy: a qualitative comparison with the Maas record. *Geomorphol. (Amst.)* 33 (3–4), 225–236. doi:10.1016/s0169-555x(99)00125-7
- Wang, C., Chen, J., and Zhang, K. (2005). Optically stimulated luminescence dating of fluvial deposits from the Mingyaoe anticline in the Southwestern Tianshan (in Chinese). *Seismol. Geol.* 27 (4), 586–598. doi:10.3969/j.issn.0253-4967.2005.04.007
- Wang, Y., and Wang, Y. (2000). Formation of the Anjihai River terraces at the north tianshan piedmont, xinjiang, and significance (in Chinese). *Geol. Rev.* 46 (6), 584–587. doi:10.3321/j.issn:0371-5736.2000.06.004
- Wegmann, K. W., and Pazzaglia, F. J. (2009). Late Quaternary fluvial terraces of the Romagna and Marche Apennines, Italy: climatic, lithologic, and tectonic controls on terrace genesis in an active orogen. *Quat. Sci. Rev.* 28 (1–2), 137–165. doi:10.1016/j.quascirev.2008.10.006
- Windley, B., Allen, M., Zhang, C., Zhao, Z., and Wang, G. (1990). Paleozoic accretion and Cenozoic reformation of the Chinese Tien Shan range, central Asia. *Geology* 18 (2), 128–131. doi:10.1130/0091-7613(1990)018<0128:paacro>2.3.co;2
- Wu, C., Zheng, W., Zhang, Z., Jia, Q., Yu, J., Zhang, H., et al. (2018). Terrace sequence along the Yushangxi River in the southern piedmont of Tian Shan and its relationship to climate and tectonics in northwestern China. *Geomorphology* 313, 48–57. doi:10.1016/j.geomorph.2018.04.009
- Yang, H., Yang, X., Huang, W., Li, A., Hu, Z., Huang, X., et al. (2020). 10Be and OSL dating of Pleistocene fluvial terraces along the Hongshuibai River: constraints on tectonic and climatic drivers for fluvial downcutting across the NE Tibetan Plateau margin, China. *Geomorphology* 348, 106884. doi:10.1016/j.geomorph.2019.106884
- Yin, A., Nie, S., Craig, P., Harrison, T., Ryerson, F., Xianglin, Q., et al. (1998). Late Cenozoic tectonic evolution of the southern Chinese Tian Shan. *Tectonics* 17 (1), 1–27. doi:10.1029/97tc03140
- Zech, R. (2012). A late pleistocene glacial chronology from the Kitschi-Kurumdu Valley, Tien Shan (Kyrgyzstan), based on 10Be surface exposure dating. *Quat. Res.* 77 (2), 281–288. doi:10.1016/j.yqres.2011.11.008
- Zech, R., Abramowski, U., Glaser, B., Sosin, P., Kubik, P. W., and Zech, W. (2005). Late Quaternary glacial and climate history of the Pamir Mountains derived from cosmogenic 10Be exposure ages. *Quat. Res.* 64 (2), 212–220. doi:10.1016/j.yqres.2005.06.002
- Zech, R., Röhringer, I., Sosin, P., Kabgov, H., Merchel, S., Akhmadaliev, S., et al. (2013). Late Pleistocene glaciations in the Gissar Range, Tajikistan, based on 10Be surface exposure dating. *Palaeogeogr. Palaeoclimatol. Palaeoecol.* 369, 253–261. doi:10.1016/j.palaeo.2012.10.031
- Zubovich, A. V., Wang, X. q., Scherba, Y. G., Schelochkov, G. G., Reilinger, R., Reigber, C., et al. (2010). GPS velocity field for the Tien Shan and surrounding regions. *Tectonics* 29 (6). doi:10.1029/2010tc002772